Cumulus Convection and the Madden-Julian Oscillation of the Tropical Troposphere

David J. Raymond
Physics Department and Geophysical Research Center
New Mexico Tech
Socorro, NM 87801

Published in Physica D, 77, 1-22, 1994.

Abstract

Parameterizations of cumulus convection for use in large scale numerical models of the atmosphere are classified according to whether they are based on an energy equilibrium principle or on a balance between the supply of mass or moisture and its consumption by convection. Though some of the most popular cumulus parameterizations are based on mass or moisture balance, I argue that energy balance is a more appropriate governing principle. Physical consistency and the absence of spurious short wavelength instabilities are points in its favor. A simple energy equilibrium parameterization with a minimal representation of precipitation processes is then described, with the objective of reducing the convective parameterization problem to its essential elements. This model is first shown not to exhibit small scale instabilities. When wave-related variations in the surface entropy flux are included, it is then found (in agreement with other energy balance models) to support large scale waves similar to the observed Madden-Julian oscillation of the tropical troposphere. The characteristic period of the waves is related to the time needed

for sea-air fluxes to alter the tropospheric profile of equivalent potential temperature, and their intensity and phase speed are sensitive to variations in the parameters controlling the formation and evaporation of precipitation.

1 Introduction

The Madden-Julian oscillation (Madden and Julian, 1971, 1972; Krishnamurti, Jayakumar, Sheng, Surgi, and Kumar, 1985; Knutson and Weickmann, 1987; Nakazawa, 1988; etc.) is a global scale equatorial wave in the tropical troposphere. It circles the earth to the east every 40 - 50 days and manifests itself particularly in the east-west or zonal wind field near the equator. The zonal wind anomaly associated with the wave changes sign between low and high levels, indicating (via mass continuity) that the wave is coupled to vertical motion in the atmosphere. As the wave strongly modulates the intensity of cumulus convection, it is one of the prime weather makers in the moist equatorial regions. In addition, it may play a role in the initiation of el Niño (Nitta and Motoki, 1987; Lau and Chan, 1988).

The Madden-Julian oscillation is arguably the simplest convectively active traveling wave disturbance in the tropical troposphere. Explaining its dynamics is important in its own right, but is also a significant step on the road to understanding more complex tropical phenomena.

Treating cumulus convection and other diabatic processes in models of large scale atmospheric flows may be characterized as a problem in statistical mechanics. Convective clouds are considered to be rather large and complex "molecules" governed by statistical laws. For sufficiently slow changes in the large scale state, convection will be in equilibrium with the environment. Determining the nature of this equilibrium is the essence of the cumulus parameterization problem.

It has long been known that deep cumulus convection is generally accompanied by large scale upward motion. A number of parameterizations of convection therefore relate the amount of convection to the strength of the large scale ascent (Ooyama, 1964; Hayashi, 1970; Lindzen, 1974). The popular parameterization of Kuo (1965, 1974) and its successors (e. g., Anthes, 1977; Molinari, 1985) are formally driven by the vertically integrated convergence of the moisture flux, or by simple variations on this theme, rather than by ascending motion, but they exhibit the same type of behavior as

those driven by ascent. The defining characteristic of these treatments of convection is that the assumed equilibrium is one that balances the moisture or mass supplied to convection by the large scale flow with the rate at which convection consumes it.

Arakawa and Schubert (1974) proposed that convection maintains a state of equilibrium with large scale convective forcing in a manner fundamentally different from that of the Kuo and related schemes. Their quasiequilibrium hypothesis states in essence that the rate of change of convective available potential energy, or CAPE[1], in the atmosphere is much slower than the individual rates of large scale production and convective destruction of CAPE[2]. The Arakawa-Schubert scheme thus postulates an equilibrium between the supply and consumption of energy rather than mass or moisture.

Hard convective adjustment (Manabe, Smagorinsky, and Strickler, 1965) is a highly simplified energy equilibrium model in which convection acts instantly to drive an unstable atmosphere to neutrality, and thus keeps the environment from developing any CAPE at all. Soft convective adjustment (Kurihara, 1973; Betts, 1986; Betts and Miller, 1986) is similar, but allows some instability to develop as a result of invoking a finite relaxation time or by choosing a target profile other than a moist adiabat or both.

Existing parameterizations of cumulus convection thus divide into two groups. In one group, equilibrium between mass or moisture supply and consumption is taken as the guiding principle, while in the other a balance between energy supply and consumption is postulated.

Mass and moisture-based cumulus parameterizations often support a kind of instability known as "wave-CISK" (e. g., Hayashi, 1970; Lindzen, 1974). CISK stands for "conditional instability of the second kind" (Charney and Eliassen, 1964) to distinguish it from the ordinary conditional instability responsible for the formation of individual cumulus clouds. It is envisioned as a cooperative instability between convection and some larger scale disturbance. Wave-CISK refers to the case when this disturbance is a large scale atmospheric wave. The energy source for modeled wave-CISK disturbances is the ambient CAPE of the atmosphere. One disturbing aspect of wave-

[1]CAPE is the work done by buoyancy forces on an ascending, nonentraining parcel in an unstable atmosphere.

[2]Actually, an extension of the concept of CAPE that includes the effects of entrainment is defined. This "cloud work function" is computed individually for each convective entrainment rate, and the work function for each entrainment category is assumed to vary only slowly with time.

CISK modes in many models is a tendency to have maximum growth rates at the shortest possible wavelengths, suggesting that the modes are nothing more than a distorted manifestation of the ordinary conditional instability responsible for the formation of individual clouds. To quote Ooyama (1982):

> The fact that cumulus parameterization does not eliminate cumulus instability has been known since Syono and Yamasaki (1966), but many papers of so-called CISK theory are discussing convective clouds in disguise. Wave-CISK ... is a typical example of such non-CISK theories in the literature.

Cumulus convection can transfer energy to large scale circulations if it releases heat preferentially in regions that are warmer at a given level than the surroundings, thus generating available potential energy, or APE[3] (Lorenz, 1955). A particularly contentious point is how and when this occurs in the tropical atmosphere. Wave-CISK models accomplish this by making convective heating occur in regions warmed by adiabatic compression created by wave-induced subsiding motions. Since neither cumulus convection nor subsidence can warm the atmosphere next to the surface[4], warming by these mechanisms necessarily increases the static stability in the lower troposphere, and therefore decreases the CAPE. Thus, for the wave-CISK mechanism to work, cumulus convection must be controlled by some factor that doesn't decrease as CAPE decreases. Mass and moisture equilibrium models can satisfy this criterion since convection is proportional to the large scale lifting or moisture convergence, independent of CAPE, as long as CAPE remains positive.

Emanuel (1986, 1987) and Xu and Emanuel (1989) have challenged the view that the CAPE of the ambient environment is needed to support large scale disturbances, and question whether such energy even exists in significant quantities in the tropics. Emanuel (1986) showed that tropical cyclones can spin up from a finite amplitude disturbance in the absence of any CAPE in the ambient atmosphere whatsoever, the actual energy source being the

[3]APE should be distinguished from CAPE. The former is the total potential and internal energy available to a flow for conversion into kinetic energy by any adiabatic rearrangement, while CAPE is the specific potential energy available to a test parcel for conversion to kinetic energy by vertical motion in moist convection.

[4]Measurements of the vertical profile of heating by deep convection, e. g., Yanai, Esbensen, and Chu (1973) typically show heating maxima in the middle to upper troposphere. Cooling (by evaporation of rain) is often found at the surface.

thermodynamic disequilibrium between the atmosphere and the sea surface. Similarly, Emanuel (1987, 1993), Neelin, Held, and Cook (1987), and Yano and Emanuel (1991) demonstrated that the Madden-Julian oscillation can be explained as a mode that draws its energy primarily or exclusively from this source.

Xu and Emanuel (1989), building on the earlier work of Betts (1982), showed that the tropical atmosphere is nearly neutrally buoyant to reversible moist parcel ascent. If convective clouds acted like nonmixing, nonprecipitating parcels, CAPE would be negative in the anomalously warm regions of wave-CISK disturbances, and convection would be energetically impossible there. Under these circumstances APE could not be generated, and wave-CISK wouldn't be possible even with a mass or moisture-based cumulus parameterization.

It seems unlikely that real convection actually behaves this way. Williams and Renno (1993) plausibly argue that convective updrafts in the real atmosphere both shed precipitation and gain additional buoyancy from freezing of liquid water, resulting in substantial CAPE being made available to a nonentraining parcel. Thus, the issue of energy transfer to the larger scale remains unresolved by this approach, though in any case the actual energy available for conversion to APE is small compared to that available from the sea surface (Randall and Wang, 1992).

A number of investigators have proposed that the Madden-Julian oscillation is a wave-CISK mode (Chang, 1977; Lau and Peng, 1987; Chang and Lim, 1988) in which the wave is an equatorially trapped Kelvin wave (Matsuno, 1966). Adiabatic Kelvin waves with a vertical scale commensurate with deep convection move much more rapidly than the observed Madden-Julian wave. Various proposals for reducing this discrepancy have been made. Typically, the wave is assumed to have its effective static stability, and hence its propagation speed, reduced by latent heat release in the updraft. However the tendency of unstable wave-CISK modes to grow most rapidly at the shortest wavelength is a more serious problem, since the Madden-Julian oscillation is manifestly a global phenomenon. If Ooyama (1982) is correct, then characterizing the Madden-Julian oscillation as a wave-CISK mode is equivalent to saying that it is just a single big cumulonimbus cloud — a demonstrably preposterous proposition!

I now argue that cumulus parameterizations with energy-based closures, such as the Arakawa-Schubert and adjustment schemes, do not allow conversion of ambient CAPE to APE, even when significant CAPE exists in

the environment. This is because the cumulus response in these schemes is typically a simple tendency to return to the equilibrium state. Anomalously warm regions necessarily have *less* convective heating, leading to the destruction of APE. Wave-CISK is not possible in these circumstances.[5] Model calculations with parameterizations of cumulus convection based on the energy equilibrium hypothesis (e. g., Stark, 1976; Neelin and Yu, 1994) have been shown not to produce wave-CISK instabilities, in agreement with this reasoning. Thus, wave-CISK modes are primarily, if not uniquely, a feature of mass and moisture equilibrium models.

The difference between mass and moisture-based models on one hand, and energy-based models on the other hand, shows up in numerical simulations. Numaguti and Hayashi (1991) have run global "aqua planet" simulations using both the Kuo cumulus parameterization (a moisture-based model) and a moist convective adjustment scheme (energy-based). Both parameterizations produce eastward-moving equatorial disturbances that have propagation speeds comparable to that of the observed Madden-Julian oscillation (Madden and Julian, 1971, 1972). However, the dominant wavelength for these disturbances is very small when the Kuo parameterization is used, a few times the grid spacing in their model. These look very much like wave-CISK modes. On the other hand, the adjustment scheme yields an eastward-propagating mode truly global in scale, with no short wave component. This result is more in keeping with observations of the phenomenon.

Emanuel's (1987) original model of the Madden-Julian oscillation is a highly simplified adjustment scheme. However, even though it is an energy-based model, it exhibits short wavelength instabilities, as seen with mass or moisture-based models. Yano and Emanuel (1991) showed that by allowing a fraction of the precipitation to evaporate and by relaxing their rigid lid boundary condition this problem is somewhat mitigated. In recent work Emanuel (1993) also showed that introducing a small lag (a few hours) in the convective response to forcing strongly suppresses short wavelength modes, leaving (mainly) eastward-propagating modes of global scale resembling the Madden-Julian oscillation.

Physical reasoning suggests that cumulus parameterizations based on en-

[5] As Emanuel (personal communication, 1993) points out, wave-CISK may be possible with traditional moist convective adjustment schemes that operate only when a relative humidity threshold is exceeded. If the large scale model has relative humidities exceeding the threshold only in anomalously warm regions, then wave-CISK may be possible. The Betts-Miller scheme mentioned above is not subject to this behavior.

ergy equilibrium are superior to those based on mass or moisture equilibrium. For instance, in an argument due to Kerry Emanuel (personal communication, 1993), imagine a horizontally homogeneous atmosphere subject to radiative cooling, with stronger cooling occurring aloft, and no surface moisture flux. Under these circumstances the vertical profile of temperature will eventually become unstable, and convection will occur. Such convection would have been predicted by an energy-based parameterization, but not by one based on mass or moisture supply, since there is no large scale ascent or moisture convergence. This calls into question the suitability of such models for representing convection in large scale calculations.

The results of Raymond (1987) suggest that wave-CISK disturbances can intensify only if they violate a fundamental relationship between convective mass flux and convective heating. In essence, even if 100% of the mass ascending through cloud base enters cumulonimbus updrafts, convective *warming* of the environment near cloud base cannot occur, and APE cannot be generated. Downdrafts can alter this argument, but in a way that prohibits large scale wave-CISK disturbances, since moisture would be used up faster than the wave could supply it. This is a violation of the equilibrium principle. Thus, even cumulus parameterizations based on mass or moisture equilibrium apparently do not support large scale wave-CISK modes if they are made consistent with the physics of convection.

The arguments presented above strongly favor the use of energy-based cumulus parameterizations. However, the current state of such parameterizations is not completely satisfactory. Most convective adjustment schemes are rather ad hoc, with the only physical content being the idea that convectively unstable fluids are driven toward convective neutrality. On the other hand, the Arakawa-Schubert scheme is too complex for use in exploratory models, and in addition uses the entraining plume model for convective cells. This model of convection is of questionable validity for shallow cumulus clouds (Raymond and Blyth, 1986; Blyth, Cooper, and Jensen, 1988; Raymond and Blyth, 1992). Emanuel (1991) has developed an energy-based parameterization that incorporates current knowledge about convection, but this model is also rather complex.

It would be desirable to have a simple cumulus parameterization based on the energy equilibrium hypothesis that retains the major physical processes in convection, even if only qualitatively. This would be extremely useful in simplified models of the atmospheric circulation. I introduce such a model in this paper. It bears some resemblance to adjustment schemes, in that

atmospheric profiles are relaxed toward target profiles. However, the model differs from these schemes in two ways: First, the variables on which the relaxation is done are not temperature and relative humidity, but equivalent potential temperature and total water mixing ratio. The first variable is related to the entropy of moist air, while the second is the mass of water vapor plus cloud water per unit mass of air. Cloud water includes droplets that are small enough to be carried along with the air, but excludes precipitation. The advantage of this choice of variables is that they are conserved or nearly conserved in many atmospheric processes.

The second major difference between the present model and most adjustment schemes is that the target profiles for these variables are not arbitrarily fixed, but are determined naturally by competing physical processes. The processes included in the model are as follows:

- Moist convection is assumed to have a tendency to conservatively drive the equivalent potential temperature and total water mixing ratio profiles toward homogeneity.

- Condensed water in saturated regions is dropped out of the atmosphere as precipitation on a very short time scale. Some of this water is reevaporated in unsaturated regions as it falls out.

- Convective precipitation is assumed to occur even in unsaturated regions, thus reducing the total water there.

- Surface fluxes of equivalent potential temperature and water are distributed through the depth of the convective layer.

These processes are implemented in the model as competing relaxation terms. There is no particular justification for this formulation aside from the imperative of simplicity. As a consequence, the model can be expected at best to yield behavior that is only qualitatively correct. Quantitative answers must be sought in more complex models. However, the successes of even simple adjustment schemes suggest that the model may have something useful to say about the real world.

The model is described in section 2. Various applicable meteorological concepts are also defined, for the benefit of nonmeteorologists. Section 3 explores some of the model's properties by examining its response to periodic vertical motion. When the wind used in surface flux calculations is held

steady, the correlation between heating and temperature anomaly is negative, as expected from the arguments presented above. Only when the horizontal surface wind is allowed to fluctuate in quadrature with the vertical wind (as would be expected in a wave-like disturbance) does the correlation become positive, and then only for periods greater than or equal to about 40 days. Section 4 presents initial value calculations of a two-dimensional numerical model of the equatorial regions with the new parameterization used to represent the effects of cumulus convection. A long period, eastward-propagating wave is found in the presence of mean easterly flow. This wave propagates at speeds comparable to the Madden-Julian wave. Variations in the rates of precipitation formation and evaporation are found to have a significant effect on wave speed and intensity. This provides a potential causal link between (possibly anthropogenic) variations in cloud microphysical processes and fluctuations in large scale atmospheric flows.

2 Model description

As noted above, the equivalent potential temperature is related to the specific entropy, s, which for a saturated or unsaturated parcel of air is given approximately[6] by

$$s = C_p \ln(T/T_R) - R^* \ln(p/p_R) + Lr_v/T_R, \tag{1}$$

where T is the temperature, p the pressure, C_p is the specific heat of air per unit mass at constant pressure, R^* is the universal gas constant divided by the molecular weight of air, L is the latent heat of condensation for water vapor, and T_R and p_R are constant reference values of temperature and pressure. The mixing ratio of water vapor, r_v, is simply the mass of water vapor per unit mass of air.

The equivalent potential temperature is defined

$$\theta_e = T_R \exp(s/C_p), \tag{2}$$

and is the temperature acquired by a parcel after a moist adiabatic expansion to very low pressure, followed by a dry adiabatic compression to the reference pressure. The equivalent potential temperature (and specific entropy)

[6]See Iribarne and Godson (1981) for an accurate expression for the specific entropy of moist air.

are precisely conserved in both moist and dry reversible adiabatic expansions and compressions. Evaporation or condensation of water doesn't change θ_e in a parcel to the extent that this process takes place reversibly. Furthermore, atmospheric motions are slow enough to be essentially reversible, so conservation is nearly perfect in the absence of radiative or mixing effects. Even mixing, which increases the entropy, is a minor nonconservative effect, since atmospheric values of θ_e have a very small dynamic range. Because of this, θ_e is said to mix almost linearly, i. e., a mixture of two parcels has an equivalent potential temperature nearly equal to the mass-weighted average of the equivalent potential temperatures of the original parcels.

The total water mixing ratio is the sum of two contributions:

$$r_t = r_v + r_c. \tag{3}$$

The water vapor mixing ratio, r_v, is defined above, while r_c is the cloud water mixing ratio, or that component of condensed water that is composed of very small drops, and is therefore effectively carried along by air motions. As saturated air rises or descends, vapor is converted to cloud water, and vice versa. However, in nonprecipitating clouds, the sum of the two, r_t, is conserved. Only when precipitation is formed or evaporates does the total water mixing ratio change in nonmixing parcels. The total water mixing ratio mixes linearly even though the individual constituents in general do not.

2.1 Parcel buoyancy

What determines the depth of the convective layer? Since little of the sun's radiation is absorbed by the earth's atmosphere[7], the surface becomes the proximate energy source for the atmosphere. Thus, with rare exception, atmospheric convection is surface-based.

The depth of the convective layer is determined locally by the vertical profile of ambient temperature and the value of equivalent potential temperature of air near the surface. The argument for this goes as follows: Since θ_e is conserved in both saturated and unsaturated adiabatic transformations,

[7]Actually, a significant fraction of solar radiation (mostly near infrared) is absorbed by water vapor in the middle troposphere (Liou, 1980). This causes a diurnal fluctuation in the intensity of convection over the ocean (Fingerhut, 1978), but doesn't fundamentally alter the arguments presented here.

it remains constant in the ascent of a nonmixing parcel. We assume that the maximum elevation clouds can reach is the upper limit of unmixed parcel ascent, and further assume that the level of neutral buoyancy for these parcels defines the depth of the convective layer. Parcels with upward velocities arriving at this layer will overshoot, but will ultimately settle there as kinetic energy is dissipated. All that remains is to determine the buoyancy of near-surface parcels as a function of height.

From (1) and (2), the equivalent potential temperature can be approximately written

$$\theta_e(T, p, r_v) = T(p_R/p)^\kappa \exp(Lr_v/C_pT_R) \tag{4}$$

where $\kappa = R^*/C_p$. The *saturated* equivalent potential temperature is defined as (4) with the saturation mixing ratio, r_s, replacing the actual mixing ratio, r_v:

$$\theta_{es}(T, p) = \theta_e(T, p, r_s). \tag{5}$$

At a given pressure level the fractional temperature difference between a parcel (subscripted p) and its environment (subscripted e) is to a good approximation

$$\frac{T_p - T_e}{T_e} = \left(\frac{\theta_{es-p} - \theta_{es-e}}{\theta_{es-e}}\right)\left(1 + \frac{LT_e}{C_pT_R}\frac{\partial r_s}{\partial T}\right)^{-1}. \tag{6}$$

Ignoring compositional effects on the density[8], this is directly proportional to the parcel buoyancy.

When a parcel is saturated, $\theta_{e-p} = \theta_{es-p}$. Thus, the level of neutral buoyancy for a saturated parcel is that level for which the parcel θ_e equals the environmental θ_{es}. When the parcel is unsaturated, the potential temperature,

$$\theta(T, p) = \theta_e(T, p, 0), \tag{7}$$

is conserved. The potential temperature is simply the temperature attained by a parcel in dry adiabatic compression or expansion to a reference pressure. Thus, $\theta_{es} = \theta \exp(Lr_s/C_pT_R)$ increases as the pressure, and hence the saturation mixing ratio, increases.

[8]In practice, the differences between the parcel and environmental water vapor and condensed water contents can have significant effects on the buoyancy in the lower to middle troposphere. These factors need to be carefully evaluated when making precise estimates of parcel buoyancy.

Figure 1 shows a plot in the $\theta_e - p$ plane of a typical atmospheric sounding over the tropical oceans. Meteorological charts of this nature are normally plotted in the $T - p$ plane, but this representation emphasizes the importance of equivalent potential temperature to parcel buoyancy. Comparing the L-shaped line representing θ_{es-p} with the right-hand curve indicating θ_{es-e} shows that the parcel experiences a small amount of negative buoyancy around its condensation level, and then positive buoyancy to about 210 mb, which is therefore the top of the convective layer.

2.2 Cumulus parameterization

Precipitation formation and evaporation have no direct effect on the equivalent potential temperature of parcels. However, thermal radiation tends to cool the troposphere at an average rate of $1 - 2$ K day^{-1}. This cooling is one of the primary links in the chain of energy transfers through the atmosphere. An important function of cumulus clouds is to carry upward the solar energy deposited at the surface.

Transfer of energy from the surface to the atmosphere is often parameterized using bulk aerodynamic approximations (see, e. g., Gill, 1982). For instance, one might write

$$F_e = \rho C(\theta_{ess} - \theta_e)U \tag{8}$$

where F_e is the vertical flux of equivalent potential temperature at some standard height just above the sea surface, ρ is the air density, θ_{ess} is the saturated equivalent potential temperature at the temperature and pressure of the sea surface, θ_e is the equivalent potential temperature at the standard height, U is the horizontal wind speed at this level, and C is a dimensionless parameter of order 10^{-3}. This formula breaks down at very low wind speed. Miller, Beljaars, and Palmer (1992) suggested using a modified formula,

$$F_e = \rho C(\theta_{ess} - \theta_e)U_e, \tag{9}$$

where $U_e = (U^2 + W^2)^{1/2}$. In general W is a complicated function of the environmental conditions, but can be expected to be of order a few meters per second. The idea is that local fluctuations of the low level wind speed of order W will occur, so that the actual wind is never zero even though a time or space average of the wind may vanish.

This equation is only valid when the sea-air temperature difference is positive. When it is negative, the atmosphere is stable just above the sea surface, and convection isn't available to carry the fluxes upward. I set $F_e = 0$ in this case.

The equations assumed to govern equivalent potential temperature, θ_e, and total cloud water, r_t, are

$$\frac{d\theta_e}{dt} = \Lambda(h-z)\left[\frac{\theta_{ess}-\theta_e}{\tau_b} + \frac{\overline{\theta}_e - \theta_e}{\tau_c}\right] + R \tag{10}$$

and

$$\frac{dr_t}{dt} = \Lambda(h-z)\left[\frac{r_{ss}-r_t}{\tau_b} + \frac{\overline{r}_t - r_t}{\tau_c}\right] - \left[\Lambda(r_t-r_s)\frac{(r_t-r_s)}{\tau_s} + \Lambda(h-z)\frac{r_t}{\tau_p} - \Lambda(r_s-r_t)\frac{(r_s-r_t)r_p}{\tau_e}\right], \tag{11}$$

where

$$\Lambda(x) = \begin{cases} 1 & \text{if } x > 0 \\ 0 & \text{otherwise} \end{cases} . \tag{12}$$

The vertical coordinate is z, time is t, R is the radiative tendency of θ_e, r_p is the mixing ratio of precipitation, r_s is the saturated mixing ratio of water vapor, r_{ss} is r_s at the sea surface temperature, and an overbar indicates an average over the depth of the convective layer, h.

Equations (10) and (11) are in the form of relaxation equations with multiple time constants and relaxation targets related to various processes. The first terms in brackets on the right sides of (10) and (11) represent sea surface fluxes of θ_e and r_t, which are assumed to be deposited in the atmosphere between the surface and the top of the convective layer. Using (9) and the related equation for water vapor fluxes, this process, which relaxes the atmosphere toward saturated sea surface values of equivalent potential temperature and water vapor mixing ratio, is easily shown to be governed by the time constant

$$\tau_b = \frac{\overline{\rho}h}{\rho_s C U_e}. \tag{13}$$

The second terms on the right sides of (10) and (11) represent the homogenizing effect of convection, and are governed by the time constant τ_c. The value of τ_c is highly uncertain, but may be estimated as follows. The time for a clear parcel to sink from the tropopause to the surface at typical

radiative cooling rates is of order 30 days. Since convection is ultimately a slave to the radiative cooling, this is also the characteristic time scale for complete overturning of the troposphere. However, because the moisture in the atmosphere has a scale height of order 3 km, vertical motions of this order are sufficient to cause a radical restructuring of the atmospheric relative humidity profile. This implies a shorter moisture adjustment time of order 4 - 6 days. For this reason I take τ_c to be of this order.

The other terms on the right side of (11) are all related to precipitation processes. The third term governs the production of precipitation in saturated regions, and has the time constant τ_s. Precipitation is generated and falls out on a time scale of much less than a day, which is essentially instantaneous for large scale models. Thus, τ_s should be as small as numerical considerations will allow.

Convective precipitation can occur even when large scale saturation does not exist. The fourth term on the right side of (11) represents the gradual depletion of total water through the depth of the convective layer, and has the characteristic time scale τ_p. This term exerts a major control over the tropospheric relative humidity, and empirical tests suggest τ_p should be of order 10 - 15 days. It is difficult to come up with an a priori estimate for τ_p.

Finally, the reevaporation of precipitation is represented by the last term on the right side of (11). This occurs only in unsaturated regions, and is proportional to the degree of subsaturation, $r_s - r_t$. The time constant is actually $\tau_e/(r_s - r_t)$, and sensible results are obtained when $\tau_e/(r_s - r_t)$ is of order a few hours for $r_s - r_t = 1$ g kg^{-1}. This causes perhaps half of the precipitation to evaporate in an environment that is unsaturated from the middle troposphere downward.

The precipitation mixing ratio obeys an equation similar to those governing θ_e and r_t. However, since precipitation falls out of the atmosphere so rapidly compared to the other time scales in the problem, the mixing ratio of precipitation can be assumed to be in equilibrium with its generation rate, allowing the time derivative and corresponding horizontal spatial derivatives to be dropped. Defining the precipitation rate, $P = \rho r_p w_t$, where w_t is the terminal fall speed of precipitation, the equation for P becomes

$$\begin{aligned} \frac{\partial P}{\partial z} \quad - \quad & \Lambda(r_s - r_t)\frac{(r_s - r_t)}{w_t \tau_e} P = \\ & -\Lambda(h - z)\frac{r_t \rho}{\tau_p} - \Lambda(r_t - r_s)\frac{(r_t - r_s)\rho}{\tau_s}. \end{aligned} \tag{14}$$

Assuming that $P = 0$ at great height, this can be integrated downward to the surface. The terminal velocity is set to the typical value for aggregated ice crystals of 1 m s^{-1} above the freezing level and to a typical raindrop fall speed of 5 m s^{-1} below the freezing level.

2.3 Radiation

The radiation term R in the equivalent potential temperature equation (10) can be written in terms of the enthalpy per unit volume and time, Q, deposited by radiation,

$$R = \frac{\theta_e}{\rho C_p T} Q = \frac{\theta_e}{\rho C_p T} (Q_{sol} + Q_{therm}), \tag{15}$$

where C_p is the specific heat of air at constant pressure, T is the temperature, and where Q has been divided into contributions from solar and thermal radiation.

The thermal radiation parameterization used here is a very simple gray body scheme. In a gray atmosphere model of thermal radiation

$$Q_{therm} = \frac{d}{dz}(I_+ - I_-), \tag{16}$$

where I_+ and I_- are the upward and downward radiative fluxes, which in the Schwarzschild-Schuster approximation obey

$$\frac{dI_+}{dz} = \rho\mu(\sigma T^4 - I_+) \tag{17}$$

and

$$\frac{dI_-}{dz} = -\rho\mu(\sigma T^4 - I_-), \tag{18}$$

where μ is the effective absorptivity of the atmosphere in the infrared and σ is the Stefan-Boltzmann constant. Subtracting these two equations results in

$$Q_{therm} = \rho\mu(2\sigma T^4 - I_+ - I_-). \tag{19}$$

Integration of (17) and (18) is subject to the conditions $I_- = 0$ at the top of the domain and $I_+ = \sigma {T_s}^4$ at the surface, where T_s is the sea surface temperature.

Solar radiation causes significant heating of both the middle troposphere and the stratosphere. Ignoring the latter effect, I approximate the middle tropospheric heating by a Gaussian profile,

$$Q_{sol} = (Q_{max}/\pi) \exp[-(z - z_{max})^2/{z_w}^2]. \tag{20}$$

The diurnal variation of solar radiation is ignored.

The free parameters of the radiation treatment are μ, the infrared absorptivity, and the solar radiation parameters, Q_{max}, z_{max}, and z_w. The values used for these parameters are listed in table 1. The parameter μ was adjusted to yield a reasonable value for the outgoing long-wave radiation in radiative-convective equilibrium. The solar radiation parameters were set to approximate the solar heating profile of Manabe and Strickler (1964).

In order to isolate the phenomena of interest here, cloud-radiation interactions are not included. Though these interactions are known to exert a major influence on tropical circulations, I ignore them in order to better focus on other effects.

3 Response of model to forced ascent

Equations (10) and (11) can be written [9]

$$\frac{d\theta_e}{dt} = \frac{\partial\theta_e}{\partial t} + w\frac{\partial\theta_e}{\partial z} = S_e \tag{21}$$

and

$$\frac{dr_t}{dt} = \frac{\partial r_t}{\partial t} + w\frac{\partial r_t}{\partial z} = S_t, \tag{22}$$

in a region of large scale vertical motion, w, where S_e and S_t are the right sides of (10) and (11). Horizontal variations in θ_e and r_t have been ignored in this approximation.

Equations (21) and (22) are solved numerically using forward differencing in time and upstream differencing in space. Though this scheme is dissipative, it is adequate for use here due particularly to the small time and space discretizations, $\Delta t = 5$ ks and $\Delta z = 1$ km. The solution procedure is to

[9] The total time derivative is taken in the context of fluid dynamics, where it means the time derivative of a variable attached to a fluid parcel. Thus, for instance, $dr_t/dt = \partial r_t/\partial t + \boldsymbol{v} \cdot \nabla r_t$, where $\boldsymbol{v}$ is the parcel velocity.

run the model to radiative-convective equilibrium, which is reliably attained by 10^4 ks (about 120 days), and then to introduce vertical motion. In order to remove high frequency oscillations associated with hunting about the equilibrium state, the solution is smoothed using a low pass time filter with a $(50\text{ ks})^{-1}$ cutoff frequency. The simulation output is then thinned to one sample every 25 ks.

3.1 Periodic forcing, fixed U_e

Wave-CISK models of tropical disturbances assume that cumulus convection adds energy to the wave by concentrating convective heating in anomalously warm regions of the wave. This process is best viewed using the energy analysis of Lorenz (1955). The potential energy per unit mass available for conversion to kinetic energy, A, referred to as the available potential energy per unit mass or APE, has the approximate form

$$A = \frac{g\theta'^2}{2\theta_0(d\theta_0/dz)} \tag{23}$$

where g is the acceleration of gravity and θ_0 is the ambient profile of potential temperature. APE is a function only of height, z, and θ', the deviation of the potential temperature from θ_0, and obeys a continuity equation

$$\frac{\partial \rho A}{\partial t} + \nabla \cdot (\rho \boldsymbol{v} A) = -\frac{g\rho w\theta'}{\theta_0} + \frac{g\rho\theta' H}{\theta_0(d\theta_0/dz)} \tag{24}$$

where $\boldsymbol{v} = (u, v, w)$ is the air velocity, ρ is the air density, and H is the time rate of change of potential temperature due to diabatic effects such as cumulus convection and radiation.

The first term on the right side of (24) represents conversion of APE to kinetic energy, while the second term represents the diabatic generation of APE. It is clear that APE is diabatically generated only when the diabatic heating and the potential temperature perturbation are positively correlated, i. e., heating must occur preferentially in those regions that are already warmer than normal.

A simple test of the viability of the wave-CISK hypothesis in conjunction with the present cumulus parameterization is to impose a periodic vertical motion and see how the parameterization responds to the forcing. If the generation rate of APE is positive, then the wave-CISK mechanism may be viable.

Parameter	Value	Comment
τ_c	333 ks	Convective relaxation time scale
τ_p	1000 ks	Convective precipitation time scale
τ_s	20 ks	Stratiform precipitation time scale
τ_e	0.005 ks	Evaporation parameter
T_s	300 K	Sea surface temperature
C	1.1×10^{-3}	Drag coefficient
U_e	5 m s^{-1}	Effective surface wind (fixed U)
W	4 m s^{-1}	Minimum surface wind (variable U)
w_0	0.003 m s^{-1}	Maximum updraft
z_t	10 km	Updraft depth
Δt	5 ks	Time step
Δz	1 km	Vertical grid step
μ	3×10^{-4} m^2 kg^{-1}	Infrared absorption coefficient
Q_{max}	0.025 K ks^{-1}	Solar heating parameter
z_{max}	3 km	Solar heating parameter
z_w	4 km	Solar heating parameter

Table 1: Values of parameters used for periodic forcing tests.

I assume that the imposed vertical velocity, w, has the form

$$w = w_0 \sin(\pi z/z_t)[1 + \sin(\omega t)]/2, \tag{25}$$

where $\omega = 2\pi/\tau_f$, for $z < z_t$, and $w = 0$ above this level. This applies periodic upward motion with the forcing period τ_f and maximum magnitude w_0 at $z = z_t/2$. This pattern has the average upward motion equal to half the maximum value, and no downward motion, and is characteristic of what might happen in a region where mean upward motion is modulated by wave disturbances.

Table 1 shows the values of parameters used for the periodic forcing tests. Runs were made for forcing periods, τ_f, of 400 ks, 800 ks, 1600 ks, and 3200 ks, or roughly 5 days to 40 days. Most importantly, U_e is taken to be constant during these tests. This is unrealistic, in that mass continuity requires there to be variations in the horizontal wind if w is nonzero. However, as wave-CISK models ignore variations in sea surface fluxes correlated with the phase of the wave, this assumption is necessary to provide a valid test of the wave-CISK hypothesis.

Figures 2a - 2c show the imposed vertical velocity, the diabatic heating rate, and the potential temperature anomaly as a function of time and height over a single oscillation period of 3200 ks or about 40 days. As is commonly seen in the tropics, the temperature anomaly is less than 1 K everywhere, even though the diabatic heating rate peaks at about 1.2 K day^{-1}. This is because the adiabatic cooling due to upward motion is very nearly in balance with the diabatic heating, only a small residual being responsible for the computed potential temperature anomaly.

Most interestingly, the correlation between the diabatic heating and the potential temperature perturbation is overwhelmingly negative. Thus, convection doesn't produce APE in this situation, it consumes it, and the wave-CISK instability cannot occur.

Figure 3 shows the wave-averaged generation rate of APE as a function of height for the four different wave periods. The generation rate of APE is negative in all cases. Since the periods of most tropical waves fall into the range of 5 to 40 days, the present cumulus parameterization does not support wave-CISK disturbances in the atmosphere. This result is consistent with the assertion in the introduction that energy-based parameterizations prohibit CISK.

3.2 Periodic forcing, variable U_e

In this subsection I relax the restriction of fixed U_e, and allow it to vary in a manner consistent with an eastward-moving wave superimposed on an easterly background flow. This is the situation in which Emanuel (1987, 1993), Yano and Emanuel (1991), and Neelin, Held, and Cook (1987) found amplifying waves identifiable with the Madden-Julian oscillation. Vertical and horizontal wind fields, w and u, are assumed to take the form

$$w = w_0[1 + \sin(\pi z/z_t)\sin(\omega t - kx)]/2 \tag{26}$$

and

$$u = U + u_0\cos(\pi z/z_t)\cos(\omega t - kx), \tag{27}$$

for $z \leq z_t$, where w_0 and u_0 are constants. The approximate mass continuity equation

$$\frac{\partial u}{\partial x} + \frac{\partial w}{\partial z} = 0 \tag{28}$$

forces a relationship between u_0 and w_0:

$$u_0 = -\frac{w_0 \tau_f c}{4 z_t}, \tag{29}$$

where $c = \omega/k$ is the phase speed of the wave relative to the atmospheric flow and τ_f is the wave period as before. Setting $x = 0$ in (26) and (27) allows the evolution of a column of air advecting with the ambient flow to be studied. Since U is the ambient wind relative to the surface, the effective wind for surface flux calculations becomes

$$U_e = \{[U - 0.25 w_0 \tau_f c \cos(\omega t)/z_t]^2 + W^2\}^{1/2}. \tag{30}$$

Setting $U = -5$ m s^{-1} and $c = 15$ m s^{-1} corresponds to a wave moving to the east at 15 m s^{-1} relative to the ambient flow, or 10 m s^{-1} relative to the surface with a 5 m s^{-1} ambient flow from the east. This is the approximate observed speed of the Madden-Julian wave.

Calculations of the response of a tropospheric column to periodic vertical motions were performed exactly as in the previous section except that U_e was allowed to vary with time according to (30). Figures 4a and 4b show the heating rate and potential temperature anomaly for $\tau_f = 3200$ ks in analogy with figures 2b and 2c. (The vertical velocity pattern, shown in figure 2a is identical for the two cases.) The temperature anomaly is in phase with the heating in this case, and generation of APE is positive. Thus, a wave of the form described by (26) and (27) will grow in amplitude with time as a result of the variation of U_e with the phase of the wave.

Figure 5 shows how the generation rate of APE varies with height and forcing period. For wave periods less than $\tau_f = 3200$ ks, the effect of variable U_e is insufficient to overcome the destruction of APE by other causes. However, for $\tau_f = 3200$ ks, or roughly 40 days, the enhancement in APE production overcomes other factors and the net production is positive. Thus a short period cutoff exists for this wave mode.

The reason for the cutoff is seen in figure 6, which shows U_e and the low level atmospheric value of θ_e as a function of the phase of the wave for various values of the forcing period. For the shorter period waves the θ_e perturbation is small and out of phase with the updraft. However for $\tau_f = 3200$ ks the equivalent potential temperature has a peak-to-peak oscillation of about 2 K and lags U_e by about a quarter of a wave period, or about 800 ks, putting it in phase with the updraft and the heating. Sections of the wave with higher surface values of θ_e exhibit greater parcel buoyancy aloft.

Why does the maximum in θ_e lag the maximum in U_e by 800 ks? The enhanced θ_e is a consequence of the stronger effective wind speed during part of the wave cycle, which causes an enhanced surface flux of θ_e. The actual maximum in θ_e is lagged from the maximum effective wind by the time required for the stronger surface fluxes to modify the atmosphere as a whole. In the cumulus parameterization, the troposphere relaxes to updated surface fluxes with the time constant τ_b, as expressed by (13). A typical value for τ_b in a deep convective regime with moderate ambient winds is 1000 ks. This is not far from the computed lag of 800 ks in this case. Thus, the characteristic time for modification of the mean tropospheric θ_e by boundary layer fluxes is the key time scale for unstable waves driven by coupled sea-air fluxes. These have been denoted WISHE modes by Yano and Emanuel (1991), for "wind-induced surface heat exchange".

To summarize, in an eastward-moving wave in an easterly mean flow, the phase lag between maximum tropospheric θ_e and the maximum sea-air flux of θ_e puts the equivalent potential temperature maximum in phase with the convective heating for wave periods of about 4×800 ks ≈ 40 day. Since higher θ_e is correlated with higher θ, APE is then generated and the disturbance amplifies. This period is in agreement with the observed period of the Madden-Julian oscillation. Thus, the WISHE mechanism provides a natural explanation for the observed time scale of this oscillation.

3.3 Importance of precipitation

The present cumulus parameterization has a number of cloud physical parameters. Varying these parameters allows the sensitivity of APE generation to changes in cloud characteristics to be tested.

Variations in the precipitation evaporation parameter, τ_e result in significant changes in the generation rate of APE. Changes in τ_e might be caused, for example, by changes in the size distribution of raindrops. At the extreme limit of $\tau_e = \infty$, APE generation is actually negative for the $\tau_f = 3200$ ks case discussed in the precious subsection, even when U_e is allowed to vary (see figure 7). The decrease in APE generation below 4 km results from the replacement of positive temperature anomalies with negative anomalies as evaporation decreases. This appears counterintuitive since evaporation tends to cool the air, but results in turn from a decrease in the amplitude of the surface θ_e oscillation, evident in comparing figure 8 to figure 6.

As figure 9 shows, the case with no evaporation of precipitation has sig-

nificantly less total sea-air heat flux, $(C_pT/\theta_e)F_e$, than the case with evaporation. The difference is greatest in the windy part of the imposed oscillation, and decreases to near zero in the low wind region.

This flux decrease is at first a mystery, as the components of F_e in (9) do not vary much between the two cases. However, recall that this expression for the flux is only valid when the sea is warmer than the immediately overlying air. When the ocean is cooler than the air, transfers are assumed to vanish in the model, since the boundary layer becomes statically stable and the convection needed to move heat and moisture away from the surface is suppressed. It turns out that the evaporation of precipitation is instrumental in keeping the air cooler than the sea surface in the model. When this evaporation is suppressed in moderate to strong wind situations, the stability of the sea-air interface becomes the primary controlling factor on surface fluxes.

The assumption that zero or negative sea-air temperature differences suppress the transfer of heat is not well tested over the ocean. Fortunately, the recently obtained flux data from the TOGA COARE experiment (Webster and Lukas, 1992) may allow us to confirm or refute this hypothesis.

The other parameter to which APE generation is sensitive is the convective precipitation time scale, τ_p. This would change in response to changes in the efficiency with which convective clouds form precipitation. Eliminating convective precipitation by setting $\tau_p = \infty$ increases the generation rate of APE, as figure 7 shows. Figure 8 reveals that the variation of the low level value of θ_e is increased for infinite τ_p, as is the total sea-air heat flux (figure 9).

When convective precipitation is turned off, the simulated atmosphere becomes considerably moister. The adjustment process drives profiles more toward a moist adiabatic than a dry adiabatic profile in this case, which, because of the less steep lapse rate, results in a cooler surface layer and less tendency to shut off surface fluxes. This underlies the above results.

4 Initial value problem

In a final series of tests, I combine the cumulus parameterization with a simple, two dimensional, nonrotating numerical model. The governing equations of section 2 are expanded to

$$\frac{\partial \theta_e}{\partial t} + u\frac{\partial \theta_e}{\partial x} + w\frac{\partial \theta_e}{\partial z} = S_e + \kappa\frac{\partial^2 \theta_e}{\partial x^2} \tag{31}$$

and

$$\frac{\partial r_t}{\partial t} + u\frac{\partial r_t}{\partial x} + w\frac{\partial r_t}{\partial z} = S_r + \kappa\frac{\partial^2 r_t}{\partial x^2}, \tag{32}$$

where u and w are the horizontal and vertical velocities, and are supplemented with the vorticity equation

$$\frac{\partial \zeta/\rho}{\partial t} + u\frac{\partial \zeta/\rho}{\partial x} + w\frac{\partial \zeta/\rho}{\partial z} = \frac{g}{\rho\theta}\frac{\partial \theta}{\partial x} + \kappa\frac{\partial^2 \zeta/\rho}{\partial x^2}, \tag{33}$$

where ζ is the vorticity normal to the $x - z$ plane, κ is an assumed constant horizontal eddy viscosity, and g is the acceleration of gravity. In the hydrostatic-anelastic approximation the vorticity definition is

$$\zeta = -\frac{\partial u}{\partial z} \tag{34}$$

and mass continuity is given by

$$\frac{\partial \rho u}{\partial x} + \frac{\partial \rho w}{\partial z} = 0. \tag{35}$$

Periodic boundary conditions are imposed at the ends of the model domain, and the calculation is assumed to be done in a reference frame that moves with the mean horizontal wind. In this frame the ocean surface moves with the opposite velocity, U_s. This velocity enters only into the calculation of surface fluxes. The model is forced for an initial interval by a localized, artificial enhancement in the effective wind, U_e.

Most models of the Madden-Julian oscillation assume it to be a Kelvin wave forced in some way by latent heat release. As Matsuno (1966) showed, the Kelvin wave solution is separable into a part representing the latitudinal dependence and a part representing the longitudinal and height dependencies. The latter part has the character of two-dimensional nonrotating flow, with the restriction that wave disturbances cannot move to the west. The above model is thus adequate to describe the essential characteristics of equatorial Kelvin waves as long as westward-moving components are suppressed.

The model is initialized by adding $U_f(x)$ to U_e, where

$$U_f(x) = U_0(1 - x^2/x_0^2), \qquad x^2 < x_0^2, \tag{36}$$

x being the dimension along the equator. This forcing was applied only for the initial time $t < t_f$, after which the resulting disturbance was allowed to freely evolve.

Parameter	Value	Comment
κ	0.05	Dimensionless viscosity
x_0	6000 km	Half-width of forcing
t_f	500 ks	Duration of forcing
U_0	4 m s^{-1}	Magnitude of forcing
U_s	5 m s^{-1}	Relative velocity of surface
wind feedback?	yes	–

Table 2: Values of parameters used for control case of two-dimensional simulation. "Wind feedback" means the feedback on the surface fluxes from wave-induced variations in the low level horizontal wind.

The domain consisted of 51 by 21 grid points with cells of dimension $\Delta x = 1000$ km in the horizontal and $\Delta z = 1$ km in the vertical. The domain size was thus 50000 km by 20 km. As in the original version, upstream differencing in space and forward differencing in time were employed, and a horizontal eddy viscosity of the form $\kappa \Delta x^2 / \Delta t$ was used, where Δt is the time step and κ is a dimensionless constant.

Table 2 shows the parameter values used in a control simulation of the Madden-Julian oscillation. The values of table 1 are also used. Figure 10 shows that the initial forcing, which is turned on for only a short time, produces an eastward-propagating wave. The speed of propagation is about 8.3 m s^{-1} relative to the fluid, or 3.3 m s^{-1} relative to the earth. The maximum updraft velocity at this level (which is near the level of peak updraft) is about 3 mm s^{-1}.

Figures 11a - 11c illustrate the spatial structure of the simulated wave at $t = 7000$ ks, when the updraft is nearly in the middle of the model domain. As figure 11a indicates, the perturbation potential temperature is nearly in the form of a plane wave with downward phase propagation above 6 km. (Recall that the wave is moving toward the east, or to the right.) The vertical component of the wavenumber is about 1 km^{-1}, which for typical dry static stabilities yields a horizontal trace speed of about 10 m s^{-1} according to hydrostatic gravity wave theory (Gill, 1982). The downward phase progression indicates upward energy propagation according to this theory, so the model results are consistent with energy generation in the convective layer and energy loss aloft. Wave energy is reflected from the upper rigid lid of the model, but the combination of weak eddy viscosity and the long round trip

time to the top of the domain and back for a gravity wave packet is sufficient to make the reflected waves insignificant in the convective layer.

Below 4 km the potential temperature perturbations are weak, and APE generation is close to zero at low levels. This is consistent with the wave being in a nearly steady state at this point, which is what is observed in figure 10.

Figure 11b shows that the horizontal wind perturbation pattern tilts to the right as well above 6 km. Maximum perturbation amplitudes are of order 2 m s^{-1} in the lower troposphere and 6 m s^{-1} in the upper troposphere. Figure 11c shows that the region of upward motion, which peaks near $x =$ 28000 km, exhibits increased values of θ_e, particularly at 1 - 2 km elevation.

The computed propagation speed of the mode of approximately 3 m s^{-1} is considerably less than the nominal observed speed of 10 m s^{-1}. However, the propagation speed is sensitive to variations in cloud physical parameters. In particular, increasing τ_e much above 0.005 ks results in no Madden-Julian oscillation in the model at all. In contrast, suppressing convective precipitation by setting $\tau_p = \infty$ increases the amplitude of the simulated Madden-Julian mode. These results are consistent with the results on the generation of APE in the previous section. Suppressing convective precipitation also increases the simulated mode's flow-relative propagation speed to 13.3 m s^{-1}, which is equivalent to 8.3 m s^{-1} relative to the earth. This is much closer to the observed speed of the Madden-Julian wave.

In order to further check the hypothesis that wave-related fluctuations in surface fluxes are responsible for the Madden-Julian oscillation, the variation in the low level wind caused by the wave is suppressed in the flux calculation. The results are shown in figure 12. A weak stationary circulation is formed by the initial forcing. This circulation persists and slowly broadens, but does not intensify with time. No hint of wave-like behavior is present in this result. Thus, variations in the surface fluxes associated with wave-associated wind speed variations seem to be needed to produce a simulated Madden-Julian oscillation in the model.

A variety of other tests were made. Of particular interest, contracting all the horizontal dimensions of the control simulation by a factor of 5 results in a simulation with no unstable wave. This supports the conclusion of the previous section that net APE production is negative for short period waves. Increasing the evaporation rate increases both the phase speed and strength of the simulated Madden-Julian oscillation.

5 Discussion

The classification of cumulus parameterizations into those based on an energy equilibrium principle and those employing a balance between mass or moisture supply and consumption turns out to be a useful distinction. In a number of analyses, the former type of model in conjunction with wind-sensitive sea surface fluxes of entropy has been shown to reproduce the Madden-Julian oscillation in numerical models as a large scale, eastward-propagating wave.

Many cumulus parameterizations based on mass or moisture balance produce very short wavelength eastward-moving modes called wave-CISK modes. They are often interpreted as a manifestation of the Madden-Julian oscillation, but evidence is mounting that these modes are nothing more than artifacts of a physically inconsistent cumulus parameterization. Mass and moisture-based schemes yield unphysical results when large scale creation of CAPE is not accompanied by environmental ascent or moistening. In addition, some of the most popular schemes of this type warm the atmosphere near cloud base. This warming is necessary for wave-CISK modes to grow, but is inconsistent with the physics of cumulus updrafts and downdrafts except on the very smallest space and time scales where equilibrium principles don't apply.

I have proposed a new energy-based parameterization in the form of an extended adjustment scheme that contains somewhat more physics than other adjustment schemes. The main advantages of this scheme are that it is posed in terms of nearly conserved variables and that it has a crude representation of the effects of precipitation. Simulations of the Madden-Julian oscillation using this parameterization yield a clear explanation for the time scale of this wave. They also suggest that the wave's strength and phase speed are sensitive to variations in the distribution of precipitation and the degree to which precipitation evaporates. The present results support the conclusion of Yano and Emanuel (1991) that the phase speed increases with decreased precipitation efficiency, i. e., with increased evaporation of precipitation. However, the two models differ on how wave strength depends on evaporation — evaporation strengthens the wave in the present model and weakens it in Yano and Emanuel's.

The interactions of clouds and radiation are neglected in this paper in preference to a focus on the effects of precipitation formation and evaporation. This is not to imply that such interactions are unimportant, merely that they are covered elsewhere. The sensitivity of the present model to

variations in precipitation processes (induced, perhaps, by variations in anthropogenic aerosol production) suggests that the dynamics of climate may be sensitive to these factors.

Acknowledgments. I have greatly benefited from many discussions with Kerry Emanuel on the subject matter of this paper. Two anonymous referees made many helpful suggestions. This work was supported by the Atmospheric Sciences Section of the National Science Foundation Grant No. ATM-8914116.

References

Anthes, R. A., 1977: A cumulus parameterization scheme utilizing a one-dimensional cloud model. *Mon. Wea. Rev.,* **105,** 270-286.

Arakawa, A., and W. H. Schubert, 1974: Interaction of a cumulus cloud ensemble with the large-scale environment, Part I. *J. Atmos. Sci.,* **31,** 674-701.

Betts, A. K., 1982: Saturation point analysis of moist convective overturning. *J. Atmos. Sci.,* **39,** 1484-1505.

Betts, A. K., 1986: A new convective adjustment scheme. Part I: Observational and theoretical basis. *Quart. J. Roy. Meteor. Soc.,* **112,** 667-691.

Betts, A. K., and M. J. Miller, 1986: A new convective adjustment scheme. Part II: Single column tests using GATE wave, BOMEX, ATEX and arctic air-mass data sets. *Quart. J. Roy. Meteor. Soc.,* **112,** 693-709.

Blyth, A. M., W. A. Cooper, and J. B. Jensen, 1988: A study of the source of entrained air in Montana cumuli. *J. Atmos. Sci.,* **45,** 3944-3964.

Chang, C.-P., 1977: Viscous internal gravity waves and low-frequency oscillations in the tropics. *J. Atmos. Sci.,* **34,** 901-910.

Chang, C.-P., and H. Lim, 1988: Kelvin wave-CISK: A possible mechanism for the 30-50 day oscillations. *J. Atmos. Sci.,* **45,** 1709-1720.

Charney, J. G. and A. Eliassen, 1964: On the growth of the hurricane depression. *J. Atmos. Sci.,* **21,** 68-75.

Emanuel, K. A., 1986: An air-sea interaction theory for tropical cyclones. Part I: Steady state maintenance. *J. Atmos. Sci.,* **43,** 585-604.

Emanuel, K. A., 1987: An air-sea interaction model of intraseasonal oscillations in the tropics. *J. Atmos. Sci.,* **44,** 2324-2340.

Emanuel, K. A., 1991: A scheme for representing cumulus convection in large scale models. *J. Atmos. Sci.,* **48,** 2313-2335.

Emanuel, K., 1993: The effect of convective response time on WISHE modes. *J. Atmos. Sci.,* **50,** 1763-1775.

Fingerhut, W. A., 1978: A numerical model of a diurnally varying tropical cloud cluster disturbance. *Mon. Wea. Rev.,* **106,** 255-264.

Gill, A. E., 1982: *Atmosphere-ocean dynamics.* Academic Press, 662 pp.

Hayashi, Y., 1970: A theory of large-scale equatorial waves generated by condensation heat and accelerating the zonal wind. *J. Meteor. Soc. Japan,* **48,** 140-160.

Iribarne, J. V., and W. L. Godson, 1981: *Atmospheric thermodynamics, 2nd Ed.* D. Reidel, 259 pp.

Knutson, T. R., and K. M. Weickmann, 1987: 30-60 Day atmospheric oscillations: Composite life cycles of convection and circulation anomalies. *Mon. Wea. Rev.,* **115,** 1407-1436.

Krishnamurti, T. N., P. K. Jayakumar, J. Sheng, N. Surgi, and A. Kumar, 1985: Divergent circulations on the 30-50 day time scale. *J. Atmos. Sci.,* **42,** 364-375.

Kuo, H. L., 1965: On the formation and intensification of tropical cyclones through latent heat release by cumulus convection. *J. Atmos. Sci.,* **22,** 40-63.

Kuo, H. L., 1974: Further studies of the parameterization of the influence of cumulus convection on large-scale flow. *J. Atmos. Sci.,* **31,** 1232-1240.

Kurihara, Y., 1973: A scheme of moist convective adjustment. *Mon. Wea. Rev.,* **101,** 547-553.

Lau, K.-M., P. H. Chan, 1988: Intraseasonal and interannual variations of tropical convection: A possible link between the 40-50 day oscillation and ENSO? *J. Atmos. Sci.,* **45,** 506-521.

Lau, K.-M., and L. Peng, 1987: Origin of low-frequency (intraseasonal) oscillations in the tropical atmosphere. Part I: Basic theory. *J. Atmos. Sci.,* **44,** 950-972.

Lindzen, R. S., 1974: Wave-CISK in the tropics. *J. Atmos. Sci.,* **31,** 156-179.

Liou, K.-N., 1980: *An introduction to atmospheric radiation.* Academic Press, 392 pp.

Lorenz, E. N., 1955: Available potential energy and the maintenance of the general circulation. *Tellus,* **7,** 157-167.

Madden, R., and P. R. Julian, 1971: Detection of a 40-50 day oscillation in the zonal wind in the tropical Pacific. *J. Atmos. Sci.,* **28,** 702-708.

Madden, R., and P. R. Julian, 1972: Description of global-scale circulation cells in the tropics with a 40-50 day period. *J. Atmos. Sci.,* **29,** 1109-1123.

Manabe, S. and R. F. Strickler, 1964: Thermal equilibrium of the atmosphere with a convective adjustment. *J. Atmos. Sci.,* **21,** 361-385.

Manabe, S., J. Smagorinsky, and R. F. Strickler, 1965: Simulated climatology of a general circulation model with a hydrologic cycle. *Mon. Wea. Rev.* **93,** 769-798.

Matsuno, T., 1966: Quasi-geostrophic motions in the equatorial area. *J. Meteor. Soc. Japan,* **44,** 25-43.

Miller, M. J., A. C. M. Beljaars, and T. N. Palmer, 1992: The sensitivity of the ECMWF model to the parameterization of evaporation from the tropical oceans. *J. Climate,* **5,** 418-434.

Molinari, J., 1985: A general form of Kuo's cumulus parameterization. *Mon. Wea. Rev.,* **113,** 1411-1416.

Nakazawa, T., 1988: Tropical super clusters within intraseasonal variations over the western Pacific. *J. Meteor. Soc. Japan,* **66,** 823-839.

Neelin, J. D., I. M. Held, and K. H. Cook, 1987: Evaporation-wind feedback and low-frequency variability in the tropical atmosphere. *J. Atmos. Sci.,* **44,** 2341-2348.

Neelin, J. D., and J.-Y. Yu, 1994: Modes of tropical variability under convective adjustment and the Madden-Julian oscillation. Part I: Analytical results. *J. Atmos. Sci.,* (in press).

Nitta, T., and T. Motoki 1987: Abrupt enhancement of convective activity and low level westerly wind during the onset phase of 1986-87 el niño. *J. Meteor. Soc. Japan,* **65,** 497-506.

Numaguti, A., and Y.-Y. Hayashi, 1991: Behavior of cumulus activity and the structures of circulations in an "aqua planet" model, Part I: The structure of the super clusters. *J. Meteor. Soc. Japan,* **69,** 541-561.

Ooyama, K., 1964: A dynamical model for the study of tropical cyclone development. *Geofisica Internacional,* **4,** 187-198.

Ooyama, K., 1982: Conceptual evolution of the theory and modeling of the tropical cyclone. *J. Meteor. Soc. Japan,* **60,** 369-379.

Randall, D. A., and J. Wang, 1992: The moist available energy of a conditionally unstable atmosphere. *J. Atmos. Sci.,* **49,** 240-255.

Raymond, D. J., 1987: A forced gravity wave model of self-organizing convection. *J. Atmos. Sci.,* **44,** 3528-3543.

Raymond, D. J., and A. M. Blyth, 1986: A stochastic mixing model for nonprecipitating cumulus clouds. *J. Atmos. Sci.,* **43,** 2708-2718.

Raymond, D. J., and A. M. Blyth, 1992: Extension of the stochastic mixing model to cumulonimbus clouds. *J. Atmos. Sci.,* **49** 1968-1983.

Reed, R. J. and E. E. Recker, 1971: Structure and properties of synoptic-scale wave disturbances in the equatorial western Pacific. *J. Atmos. Sci.,* **28,** 1117-1133.

Stark, T. E., 1976: Wave-CISK and cumulus parameterization. *J. Atmos. Sci.,* **33,** 2383-2391.

Syono, S., and M. Yamasaki, 1966: Stability of symmetrical motions by latent heat released by cumulus convection under the existence of surface friction. *J. Meteor. Soc. Japan,*, **44,** 353-375.

Webster, P. J., and R. Lukas, 1992: TOGA COARE: the TOGA coupled ocean-atmosphere response experiment. *Bull. Am. Meteor. Soc.,* **73,** 1377-1416.

Williams, E., and N. Renno, 1993: An analysis of the conditional instability of the tropical atmosphere. *Mon. Wea. Rev.,* **121,** 21-36.

Xu, K.-M., and K. A. Emanuel, 1989: Is the tropical atmosphere conditionally unstable? *Mon. Wea. Rev.,* **117,** 1471-1479.

Yanai, M., S. Esbensen and J. H. Chu, 1973: Determination of bulk properties of tropical cloud clusters from large scale heat and moisture budgets. *J. Atmos. Sci.,* **30,** 611-627.

Yano, J.-I., and K. Emanuel, 1991: An improved model of the equatorial troposphere and its coupling with the stratosphere. *J. Atmos. Sci.,* **48,** 377-389.

Figures

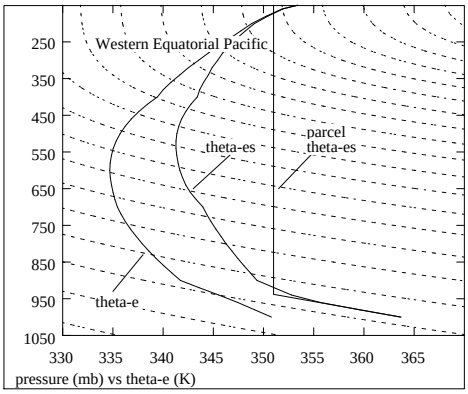

Figure 1: Plot of mean sounding from the western equatorial Pacific (Reed and Recker, 1971) in the $p - \theta_e$ plane. The left and right solid curves are the equivalent potential temperature, θ_e, and the saturated equivalent potential temperature, θ_{es}, of the environment. The dashed lines are contours of constant potential temperature, θ. The L-shaped line indicates the θ_{es} of a lifted surface parcel, the kink showing where the parcel reaches its lifting condensation level. The difference between this line and the environmental θ_{es} is proportional to parcel buoyancy.

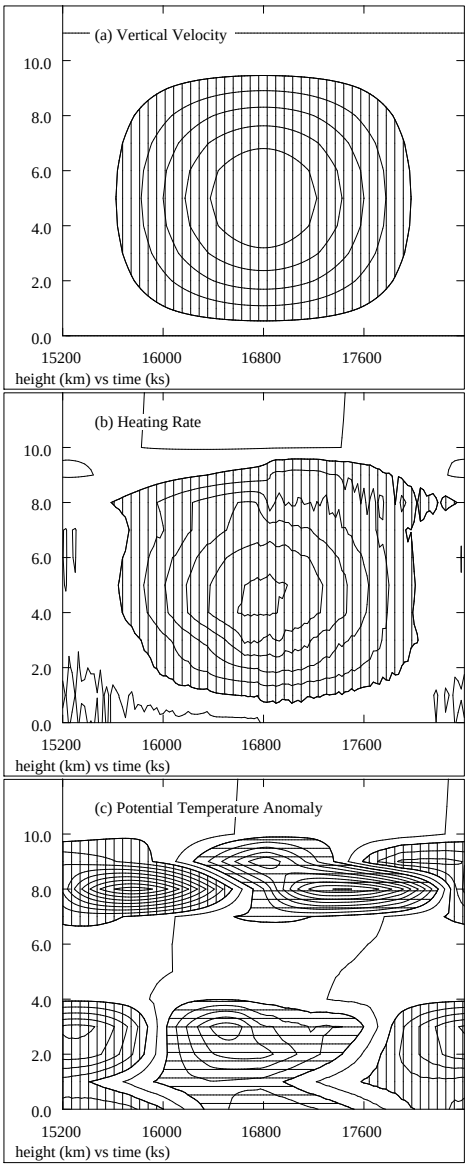

Figure 2: Plots of various fields as a function of height and time over a period of one wave cycle for periodic forcing with U_e constant. The period is $\tau_f = 3200$ ks or about 40 days. (a) Vertical velocity, w. The contour interval is 0.5 mm s^{-1}, and vertical hatching indicates upward velocities exceeding this value. (b) Diabatic heating rate. The contour interval is 0.2 K day^{-1}, and heating rates greater than this value are indicated by vertical hatching. (c) Potential temperature anomaly, θ'. The contour interval is 0.1 K. Vertical hatching indicates $\theta' > 0.1$ K, while horizontal hatching indicates $\theta' < -0.1$ K.

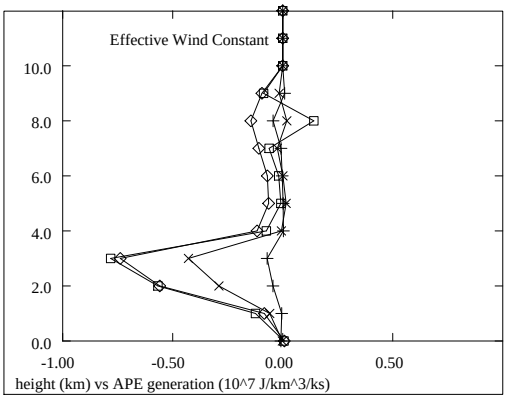

Figure 3: Generation rate of APE as a function of height in simulations with periodic forcing and fixed U_e for four different forcing periods, 400 ks (pluses), 800 ks (crosses), 1600 ks (squares) and 3200 ks (diamonds). Note that the generation rates are negative for all cases.

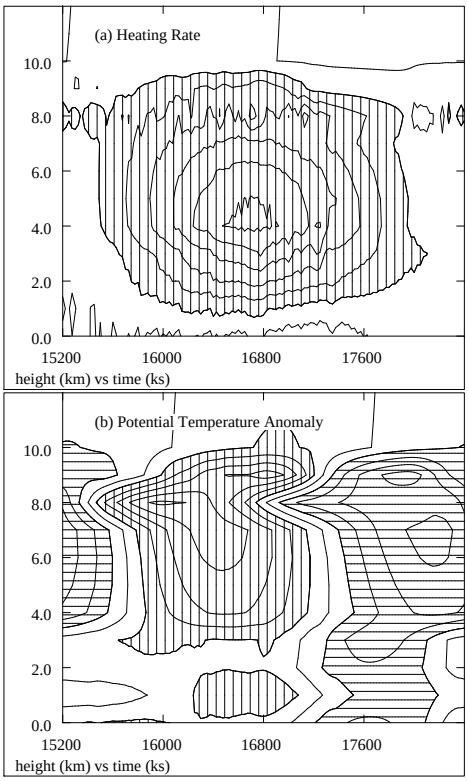

Figure 4: Plots of various fields as a function of height and time over a period of one wave cycle for periodic forcing with variable U_e. The period is $\tau_f = 3200$ ks or about 40 days. (a) Diabatic heating rate. The contour interval is 0.2 K day^{-1}, and heating rates greater than this value are indicated by vertical hatching. (b) Potential temperature anomaly, θ'. The contour interval is 0.2 K. Vertical hatching indicates $\theta' > 0.2$ K, while horizontal hatching indicates $\theta' < -0.2$ K.

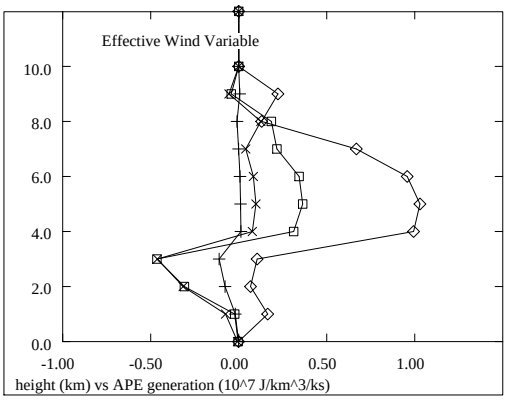

Figure 5: Generation rate of APE as in figure 3, except variable U_e.

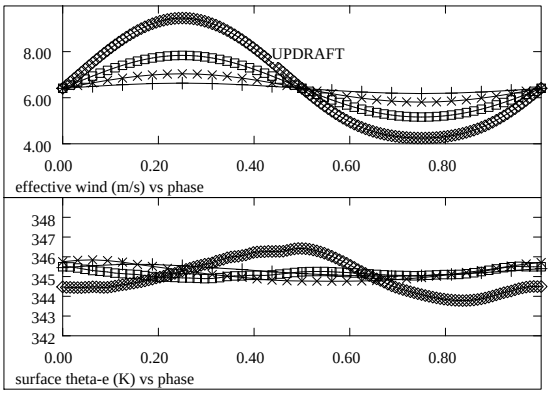

Figure 6: Effective wind, U_e, and surface θ_e as a function of wave phase for the simulations with variable U_e. One wave period is shown for each of four different values of τ_f, 400 ks (pluses), 800 ks (crosses), 1600 ks (squares), and 3200 ks (diamonds). The updraft is centered where the phase equals 0.5.

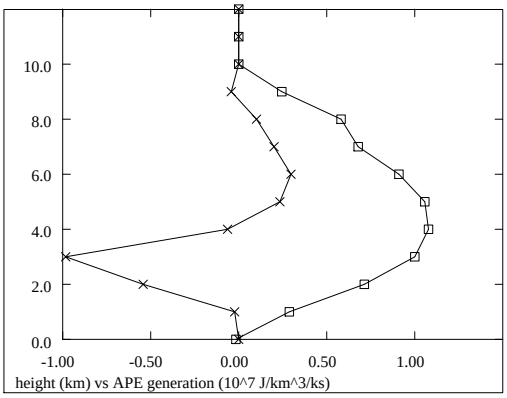

Figure 7: Generation rate of APE as in figure 5, except $\tau_f = 3200$ ks only. Two cases are shown, evaporation of precipitation suppressed (crosses) and convective precipitation suppressed (squares).

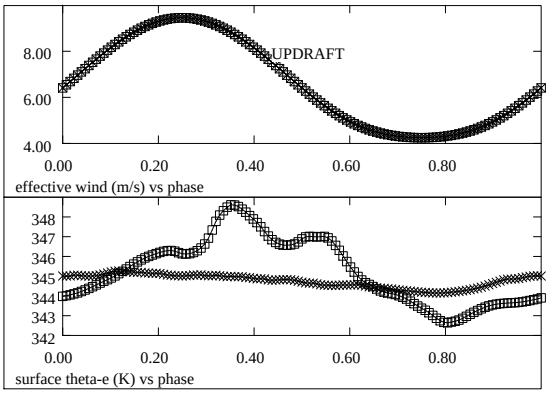

Figure 8: As in figure 6, except $\tau_f = 3200$ ks only. Two cases are shown, evaporation of precipitation suppressed (crosses) and convective precipitation suppressed (squares).

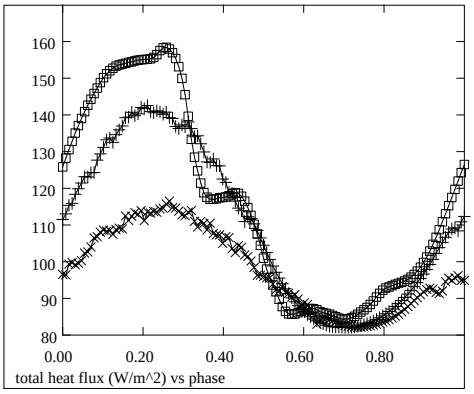

Figure 9: Total sea-air heat flux as a function of the wave phase for three cases, with the evaporation of precipitation suppressed (crosses), with convective precipitation suppressed (squares), and the control case with both of these processes turned on (pluses). All three cases have $\tau_f = 3200$ ks

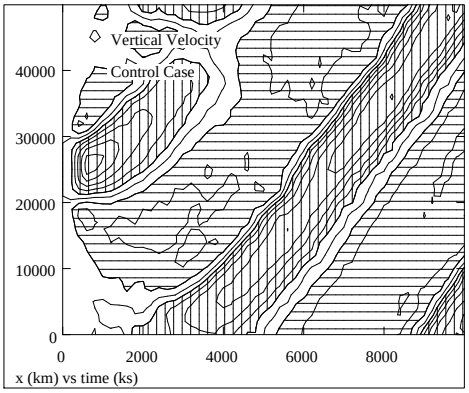

Figure 10: Vertical velocity at $z = 5$ km in $x - t$ plane for control simulation. The contour interval is 0.5 mm s^{-1}. Vertical hatching shows regions with $w > 0.5$ mm s^{-1}, while horizontal hatching indicates $w < -0.5$ mm s^{-1}.

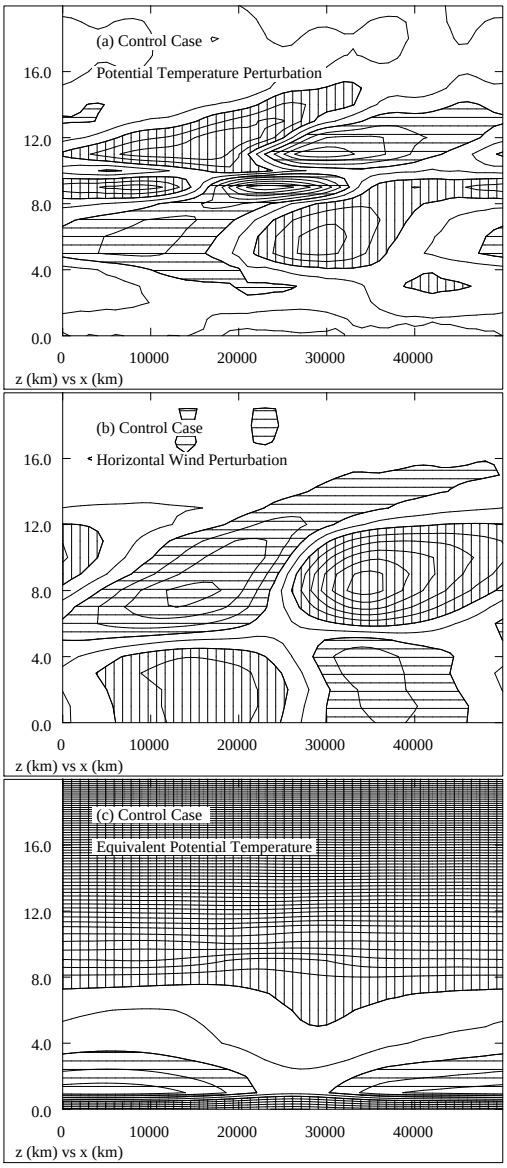

Figure 11: Plots in the $x-z$ plane of various fields at $t = 7000$ ks for the control simulation. (a) Deviation of potential temperature from horizontal mean. The contour interval is 0.2 K. Vertical hatching indicates values greater than 0.2 K, while horizontal hatching indicates values less than -0.2 K. (b) Horizontal wind relative to the ambient flow. The contour interval is 1 m s^{-1}, with vertical hatching indicating values greater than 1 m s^{-1} and horizontal hatching indicating values less than -1 m s^{-1}. (c) Equivalent potential temperature. The contour interval is 2 K, with vertical hatching indicating values greater than 348 K and horizontal hatching indicating values less than 344 K.

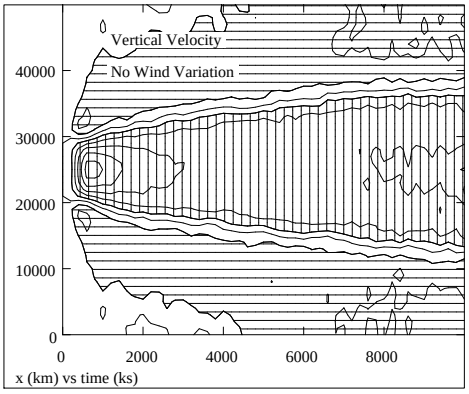

Figure 12: Vertical velocity as in figure 10, except with the wave-associated variations in horizontal wind suppressed in the surface flux calculations.